Diffusion Measurements of Hydrocarbons in Zeolites with Pulse-Field Gradient Nuclear Magnetic Resonance Spectroscopy

V. V. Zhivonitko[a], Z. Vajglová[b], P. Mäki-Arvela[b], N. Kumar[b], M. Peurla[c], and D. Yu. Murzin[b],*

[a] NMR Research Unit, University of Oulu, Oulu, Finland
[b] Johan Gadolin Process Chemistry Centre, Åbo Akademi University, Turku, Finland
[c] Laboratory of Electron Microscopy, University of Turku, Turku, Finland
***e-mail: Dmitry.Murzin@abo.fi**

Abstract—Pulse field gradient NMR technique was used to determine self-diffusivity of heptane and pentadecane at room temperature for microporous catalysts, used both as powders and shaped with a binder extrudates. The results showed that diffusivities increased with increasing specific surface area, micro- and mesopore volume of the studied catalysts. The presence of Bindzil binder together with H-Beta-25 decreased hydrocarbon diffusivities. Self-diffusivities of heptane and pentadecane were smaller for extrudates than for the powder catalysts. The detailed information about mass transfer limitations is needed to further process optimization since effective diffusivity is directly correlated with self-diffusion coefficients. The estimates of the ratio of porosity and tortuosity were also determined. The diffusion measurements with relatively long observation times Δ (20 up to 1000 ms) and catalysts fully immersed in pentadecane revealed that a small portion of sites exhibits very small diffusivities in H-Beta-25-Bindzil extrudates, which is correlated with a low ratio of mesopore to micropore volumes of this material.

1. INTRODUCTION

Acidic zeolites and their metal modified counterparts are important catalysts in many areas including oil refining and synthesis of bio-fuels via hydrocracking of long chain alkanes [1, 2]. It has already been shown that especially hierarchical mesoporous zeolites are very promising catalysts in hydrocracking of hexadecane; with increase in mesoporosity, the product distribution in hydrocracking of hexadecane can be increased [3]. Hydrocracking processes are performed industrially in fixed bed reactors [4]. A current trend in fine chemicals industry is to switch from batch to continuous operation. In this context a comparative work of using powder and extrudate catalysts was performed in [1, 5–8] focusing especially on the effect of acidity and metal dispersion in the synthesis of menthol [5].

In order to optimize industrial continuous processes in oil refining or production of fine chemicals and to maximize the desired product yields, it is important to know diffusivities of different feedstock molecules in the catalysts, which often are extrudates [9]. Pulsed-field gradient NMR (PFG NMR) method has been used to determine self-diffusivities of hydro-

carbons in mesoporous silica MCM-41 [10] and in silicalite-1 [11–13]. In addition, this technique has already been applied for MFI-type zeolites in a wide temperature range [14]. PFG NMR method facilitates in depth studies of mass transfer in heterogeneous catalysts giving information about the average diffusion path length in a given time interval (Δ) that is set in an employed pulse sequence [15]. The effective intracrystalline self-diffusivity D can be determined from the Einstein equation [15] in which the mean square displacement $\langle r^2(\Delta) \rangle$ for three-dimensional case is given as a function of time as follows:

$$\left\langle r^2(\Delta) \right\rangle = 6D\Delta, \tag{1}$$

in which Δ is the observation time. Practically, Δ is the separation between two pulsed-field gradients or between two pairs of bipolar pulsed-field gradients that encode molecular displacements. The root mean square displacement, $\langle r^2(t) \rangle^{1/2}$ varies typically between 0.4 to 3.5 μm [11], but can be larger to probe the long time limit diffusion coefficients.

In this work, the emphasis is on determination of the diffusion coefficients for heptane and pentadecane in different zeolites using PFG NMR technique.

According to our knowledge this method was applied only in [9] for assessment of effective diffusivity in technical zeolite bodies based on ZSM-5. Comparison of effective diffusivity of hydrocarbons in powder and extrudates catalysts could give some insights when correlating the catalytic results in a fixed bed operation with the properties of materials. This work gives a comparative determination of diffusion coefficients in different micro- and mesoporous catalysts, both in powder and extrudate forms for heptane and pentadecane with the PFG NMR technique. The selection of probe molecules is related to their applications in industry. Heptane diffusion is interesting because heptane isomerization was studied in Pt, Ni, Co, Fe, Cr, Pt-Cr catalysts using extrudates of H-ZSM-5, H-Beta-25, H-Y-5, CBV, SK, UX with an alumina or a bentonite clay binder [16–18] as a part of the hydroisomerization process improving the octane number. Pentadecane on the other hand is a model compound representing so-called renewable diesel, which is produced by hydrotreating of fatty acids and their derivatives. As a part of this technology, skeletal isomerization of long chain hydrocarbons with the carbon number similar to pentadecane is performed industrially in the presence of hydrogen to improve the cold flow properties of renewable diesel. Diffusion coefficients of pentadecane and heptane were determined in the following catalytic materials: (**1**) Bindzil, which is a binder in the synthesis of extrudates [6], (**2**) H-Beta-25 (in which 25 denotes SiO_2 to Al_2O_3 ratio), (**3**) mixture of H-Beta-25 powder with 30 wt % Bindzil, and (**4**) the corresponding H-Beta-25–30 wt % Bindzil extrudates. These results were correlated with transmission and scanning electron microscopy, nitrogen physisorption data and pyridine adsorption with FTIR to determine catalyst acidity.

2. EXPERIMENTAL

2.1. Preparation of Zeolite Catalysts

A commercial NH_4-Beta-25 zeolite from Zeolyst International (CP814E, $SiO_2/Al_2O_3 = 25$) was transformed to the corresponding proton form (H-Beta-25) and calcined at 500°C [8]. Bindzil-50/80 (50% colloidal SiO_2 in H_2O from Akzo Nobel) was selected as a binder. All materials were used as powders (below <63 μm). Extrudates were prepared using the weight ratio of the zeolite to the binder of 70/30 as a suspension for extrusion and catalyst shaping [5–7, 19]. A colloidal silica binder in the suspension form (Bindzil-50/80) was directly added into the water solution of grinded H-Beta-25. The weight ratio of the slurries for the extruder was 44.5/54.5/1 of the composite materials (i.e., H-Beta-25 with a binder/distilled water/methylcellulose). The extrudates were shaped in the one-screw extrusion device (TBL-2, Tianjin Tianda Beiyang Chemical Co. Ltd., China) into the cylindrical bodies with a diameter of 1.5 mm and cut to

a length of ~10 mm. The samples were denoted as Bindzil-50/80 (**1**), H-Beta-25 (**2**), H-Beta-25–30 wt % Bindzil (P) (**3**) and H-Beta-25–30 wt % Bindzil (E) (**4**), where P stands for powder and E for extrudates.

2.2. Characterization of Zeolite Catalysts

Specific surface area, pore volume and pore size distribution were determined by nitrogen physisorption using Micromeritics 3Flex-3500. Catalyst crystallite size and shape were analyzed by transmission electron microscopy (TEM, JEOL JEM-1400Plus). The surface morphology, catalyst particle size and chemical catalyst-binder interaction were studied by scanning electron microscopy (SEM, Zeiss Leo Gemini 1530).

The quantity of Brønsted and Lewis acid sites was determined by pyridine adsorption with Fourier transform infrared spectroscopy using an ATI Mattson instrument. Pyridine (Sigma-Aldrich, >99.5%) was absorbed on the thin self-supporting catalyst wafer for 30 min at 100°C followed by desorption at 250, 350, and 450°C for 1 h and the spectra of the catalysts were recorded at these temperatures. Brønsted- and Lewis-acid sites were quantified using spectral bands at 1545 and 1450 cm^{-1}, respectively using the molar extinction coefficients of Emeis [20].

2.3. Pulse-Field Gradient NMR Determination of Diffusion Coefficients

Diffusion measurements were performed on a Bruker 400 MHz spectrometer equipped with magnetic field gradient accessories. The Cotts's 13 interval PFG stimulated spin-echo with bipolar gradients [21] was used in the experiments. The samples were prepared by immersion of zeolite materials in pure pentadecane (>99%, Aldrich) or heptane (>99%, TCI) followed by evacuation of air bubbles from the materials and removing the excess solvent by rolling over filter paper. In the case of heptane, the latter procedure needs to be done rapidly to avoid drawing liquid from the pores. The saturated materials were then transferred to sealed 5 mm NMR sample tubes for analysis. Selected H-Beta-25 materials were studied also without removing the access of the solvents for the sake of comparison. Laplace inversion [22–24] was used to analyze the results in those cases.

The experiments were performed with 2 ms gradient pulses by varying the gradient strength. Relatively long observation times Δ (20 and 200 ms) were used to assess the effective diffusion coefficients at the long-time limit and to be closer to the short gradient pulse approximation. Both values provided quite similar diffusion coefficients, confirming their time independence, as it should be at the long-time limit. The initial part of the echo attenuation curves was used to obtain mean square displacements, which is equal to determining the second moment of the average diffu-

Table 1. Textural properties and catalyst particle size determined by TEM and SEM

Sample	A, m²/g	V_p, cm³/g	V_μ, cm³/g	V_m, cm³/g	V_m/V_μ	d_p, nm	d_μ, nm	d_m, nm	d_{TEM}, nm	d_{TEM} (min−max), nm	d_{SEM}, nm	d_{SEM} (min−max), nm
1 (P)	157[a]	0.30	0.01	0.29	29	—	—	2.9	30	6−158	47	15−285
2 (P)	736[b]	0.96	0.26	0.70	2.7	0.73	0.66	3.2	14	9−29	85	1.5−386
3 (P)	478[b] (562)	0.68 (0.76)	0.17 (0.19)	0.51 (0.58)	3.0	0.69	0.66	3.8	16	7−98	86	29−576
4 (E)	481[b] (562)	0.60 (0.76)	0.17 (0.19)	0.43 (0.58)	2.5	0.70	0.66	3.8	15	8−73	77	24−624

Designation: P—powder catalyst, fraction <63 µm; E—extrudates, size 1.5 × 10 mm; [a]BET method; [b]Dubinin−Radushkevich method; theoretical value in brackets was calculated from the contribution of non-agglomerated neat components in the powder form; A—specific surface area; V_p—specific pore volume; V_μ—micropore volume (<2 nm); V_m—mesopore volume (2−50 nm); d_p — median pore width; d_μ—micropore size at maximum; d_m—mesopore size at maximum; d_{TEM}—median particle size determined by TEM; d_{SEM}—median particle size determined by SEM.

sion propagator [22]. Pure unrestricted pentadecane ($D^0 = 3.8 \times 10^{-10}$ m²/s) and heptane ($D^0 = 2.7 \times 10^{-9}$ m²/s) were used as references.

The diffusion measurements were performed at 25°C, while hydroisomerization of long-chain paraffins [1] and heptane isomerization [25] are typically performed at 250 and 190−270°C, respectively. The room temperature measurements for self-diffusion give qualitative information about the order of diffusivities in a physically mixed powder and extrudates. Since the order of diffusion coefficients in different catalysts will not change with increasing temperature, these data can be correlated with the catalytic results. Furthermore, effective diffusivity is directly correlated with the self-diffusion coefficient giving an order of magnitude to the effective diffusion coefficient. The latter is essential in assessing mass transfer limitations in the catalytic reaction as will be discussed below. Recycling delays and spin-echo times were optimized by taking inversion-recovery and CPMG measurements, respectively.

3. RESULTS AND DISCUSSION

3.1. Catalyst Characterization Results

Relatively low values of specific surface area (157 m²/g) and total pore volume (0.3 cm³/g) were obtained for mesoporous Bindzil binder (**1**) with a broad range of pore size (Table 1, Fig. 1). About 5-fold higher specific surface area and about 3-fold higher specific pore volume were determined for H-Beta-25 (**2**) (736 m²/g, 0.96 cm³/g) neat powder catalyst containing about 30% of micro- and 70% of mesopores volume (Table 1). The pore size distribution of H-Beta-25 (**2**) shows a narrow range of micro-pore diameter only with one maximum and a broad range of mesopore diameter (Fig. 2). The median pore width of H-Beta-25 (**2**) was 0.7 nm (Table 1). As was expected, for powder composites and extrudates containing 70 wt % of the catalyst and 30 wt % of binder, lower values of textural properties were observed compared to the neat powder catalyst (Table 1). The theoretical

value of the surface area and pore volume (calculated from the contribution of non-agglomerated neat components in the powder form) was 20% and by up to 27% higher, respectively. These differences from the theoretical values are in line with the literature [6−8] and can be attributed to the interphases interactions observed in SEM images (Fig. 3).

SEM images and particle size distribution (Fig. 3, Table 1) also show that particles and their agglomerates were the smallest for Bindzil binder (**1**) while for neat H-Beta-25 (**2**) the median particle size was about two-fold higher and the particle size distribution was broader. In the case of the composite (**3**) and extrudates (**4**) small unpredictable changes in the particle size distribution were observed due to agglomeration of the catalyst with the binder and application of the mechanical force during extrusion.

Contrary, TEM images (Fig. 4) confirmed that these steps of catalyst preparation did not damage the crystalline shape and size of the individual material, i.e., a regular round crystalline shape of Bindzil binder (**1**) [6], and an irregular circular, elliptical crystalline shape of H-Beta-25 (**2**) [6−8] catalyst. At the same time, for the composite (**3**) and extrudates (**4**), the crystalline size slightly increased in average giving also a broader distribution with a shift to a larger particle sizes due to the presence of 30 wt % Bindzil binder with a bigger part of a larger crystallites compared to the neat catalyst (**2**) (Table 1, Fig. 4).

The results from acidity measurements for different catalysts are shown in Table 2. The Bindzil binder exhibited very low acidity, and the strongest Brønsted acidity was obtained for the parent H-Beta-25. Brønsted acidity of **3** was higher than for the parent H-Beta-25, **2**. It was, however, interesting to observe that Brønsted acidity of the extrudate **4** was higher than for the powder **3**. Lewis acidity was also the highest for H-Beta-25-P. The concentration of Lewis acidity for samples **3** and **4** were the same, opposite to the case for Brønsted acidity.
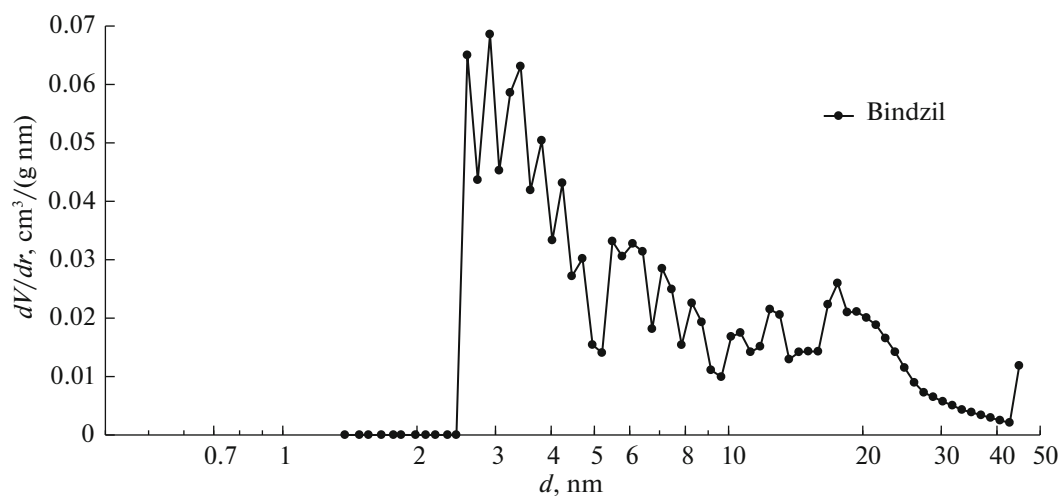
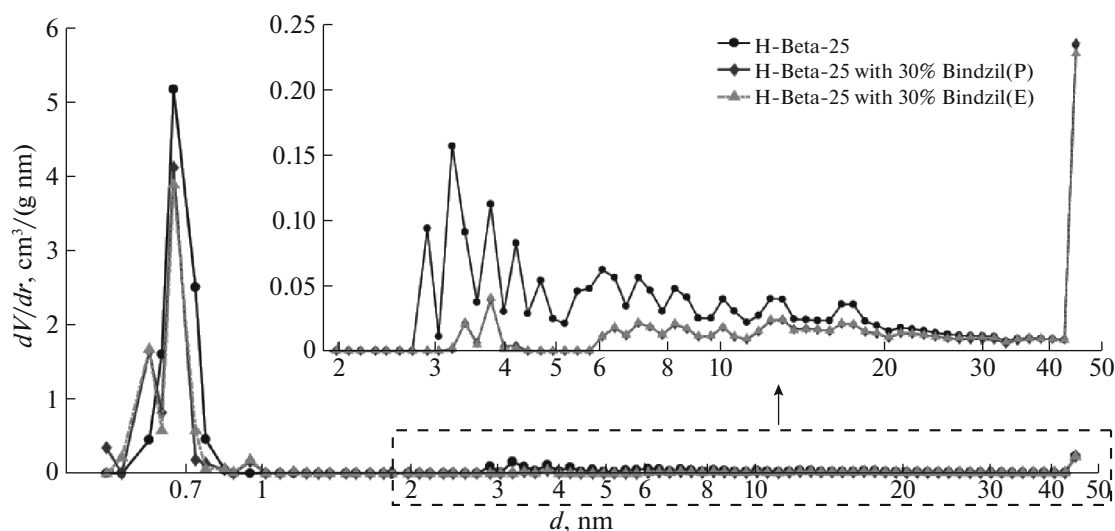**Fig. 1.** Pore size distribution: Bindzil.

Fig 2. Pore size distribution: H-Beta-25 (circle); H-Beta-25−30 wt % Bindzil powder (diamond); H-Beta-25−30 wt % Bindzil extrudates (triangle).

3.2. Results from Diffusivity Measurements with PFG NMR Method

Results from diffusion measurements of pentadecane for catalysts are depicted in Fig. 5, which shows that pentadecane diffusivity is 1.7 fold higher for the parent H-Beta-25 than for Bindzil (Fig. 5, sample **2** in comparison to sample **1**). A slightly lower diffusivity value for pentadecane was also found for H-Beta-25−30 wt % Bindzil extrudates in comparison to its powder form (Fig. 5, samples **3** and **4**). It was also stated in

**Table 2.** Acid site concentrations for different catalysts determined by pyridine adsorption

Sample	Brønsted acidity, μmol/g				Lewis acidity, μmol/g				Total acidity
	weak	medium	strong	Σ	weak	medium	strong	Σ	μmol/g
1 (P)	0	0	1	1	1	0	0	1	2
2 (P)	53	42	191	287	35	17	10	63	349
3 (P)	34	55	41	131	25	3	2	30	161
4 (E)	50	17	77	145	25	2	2	30	175
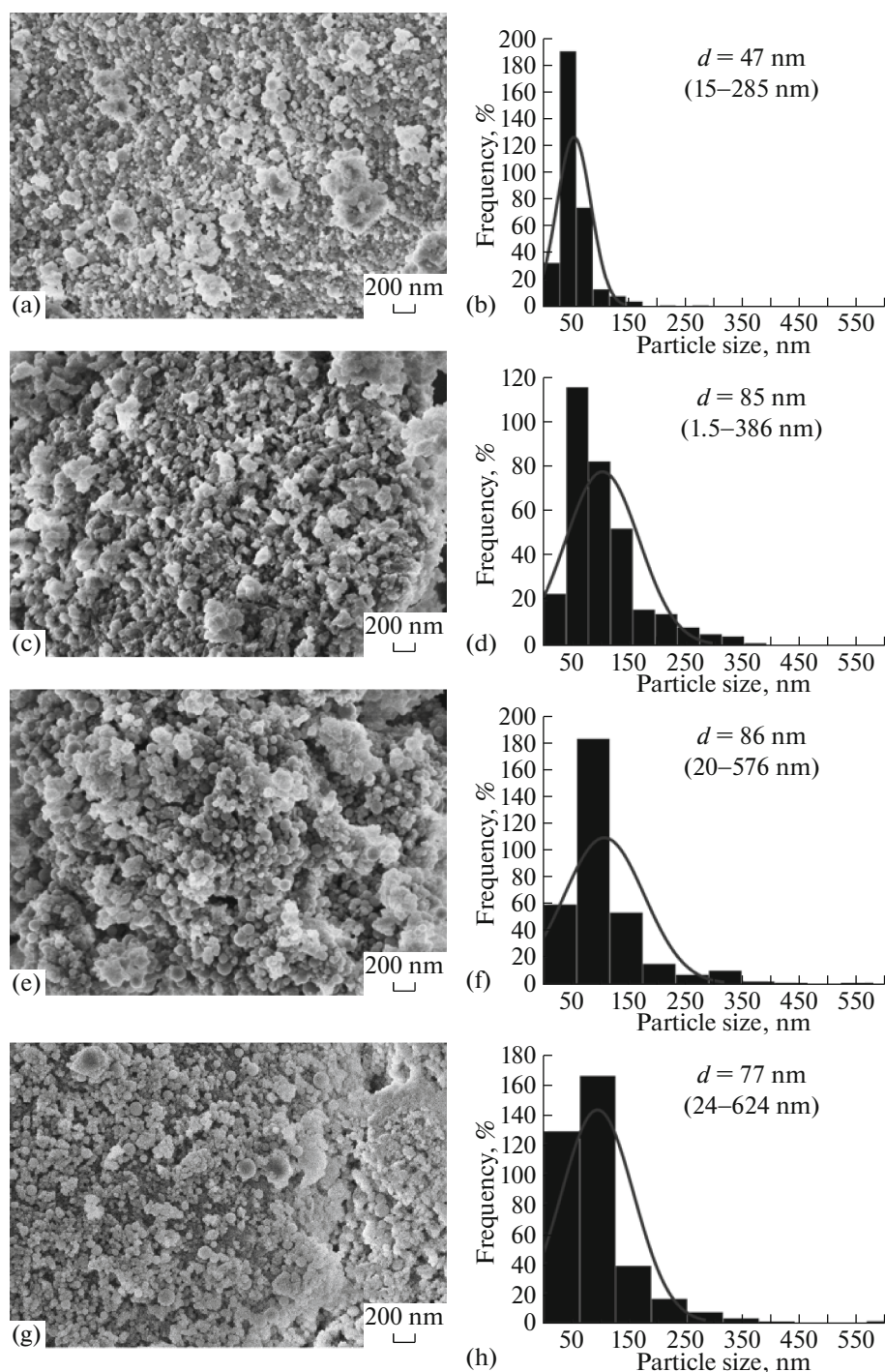
Fig. 3. SEM -images and particle size distribution: (a, b) Bindzil; (c, d) H-Beta-25 (P); (e, f) H-Beta-25–30 wt % Bindzil powder; and (g, h) H-Beta-25–30 wt % Bindzil extrudates.

[9] that for extrudates much smaller diffusivity values can be obtained in the binder part in comparison to microporous zeolite constituent of the extrudates. Furthermore, it was expected that the presence of the binder can diminish microporosity [9]. Moreover, hexane and pentadecane data cannot be compared quantitatively also because of a significant difference in the molecular size.

The diffusion coefficients for heptane for the same catalysts as studied for pentadecane diffusivity are shown in Fig. 6. The highest heptane diffusion coefficient was observed for H-Beta-25 (Fig. 6, sample **2**). It should, however, be pointed out that the sample preparation for H-Beta-25 is different than the one used for measurements of the diffusion coefficients for pentadecane. The liquid heptane between catalyst
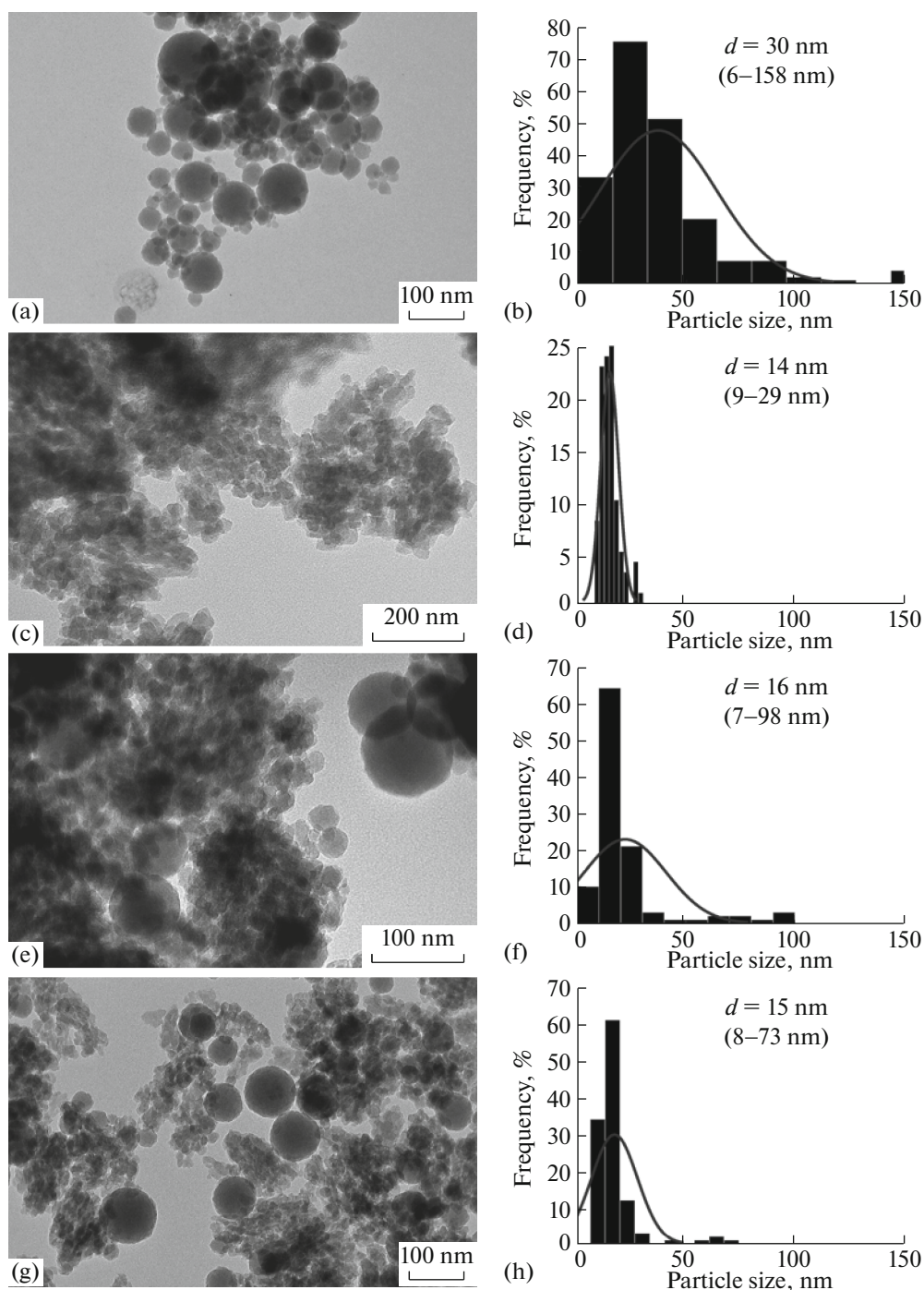
Fig. 4. TEM images and particle size distribution: (a, b) Bindzil (data from [6]); (c, d) H-Beta-25 (P); (e, f) H-Beta-25−30 wt % Bindzil powder, and (g, h) H-Beta-25−30 wt % Bindzil extrudates.

particles/beads was not removed, because this was not possible to do without drawing heptane from the pores of the material. Therefore, the corresponding D value is an overestimation of the true diffusion coefficient. The order of magnitude of the measured diffusivities is in good agreement with [9] reporting the measured diffusion coefficients of alike hydrocarbons in zeolites

of ~10^{-9} cm²/s. Very high diffusivities were reported with small crystals, while aggregation of small crystals leads to retardation of diffusion [26]. No correlation with diffusivity and the catalyst particle sizes were observed in the current work.

The diffusivity for heptane in the current work was also ~7 times higher than for pentadecane, which can
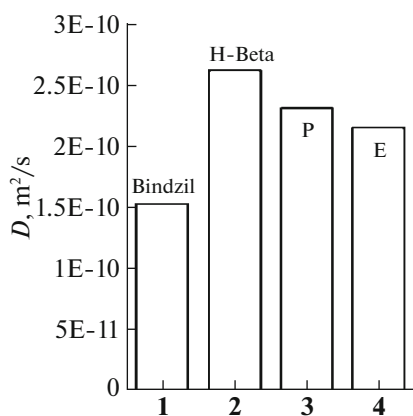
Fig. 5. Pentadecane self-diffusion coefficients according to PFG NMR measurements at long diffusion time limit in the diffusion time range of 20−200 ms. Long-time limit characterizes the pore connectivity and molecular transport inside beads of the material (root mean square displacement is on the order of ten μm). Notation: (**1**) Bindzil, (**2**) H-Beta-25, (**3**) H-Beta-25−30 wt % Bindzil powder, and (**4**) H-Beta-25−30 wt % Bindzil extrudates.
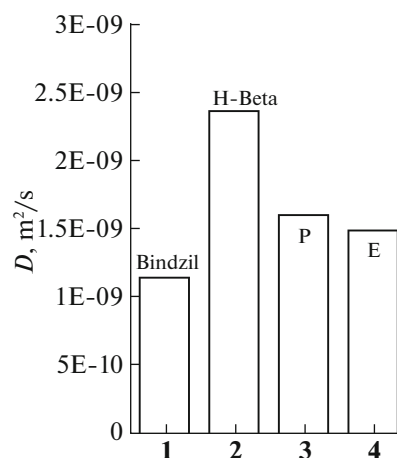
Fig. 6. Heptane self-diffusion coefficients according to PFG NMR measurements at long diffusion time limit in the diffusion time range of 20−200 ms. Long-time limit characterizes the pore connectivity and molecular transport inside beads of the material (root mean square displacement is on the order of ten μm). Notation: (**1**) Bindzil, (**2**) H-Beta-25, (**3**) H-Beta-25−30 wt % Bindzil powder, and (**4**) H-Beta-25−30 wt % Bindzil extrudates.

be explained naturally by a larger size of pentadecane. The kinetic diameter of heptane is 0.43 nm [27], while cross section of pentadecane according to ChemDraw 5.0 is 1.1 nm. When comparing diffusivity values of different alkanes in microporous silicalite-1 with the pore size of 0.55 nm [11], it was observed that diffusivity values decreased by 0.4 m^2/s at room temperature when increasing by one carbon in the hydrocarbon chain. The order of diffusivity values with different materials follows an analogous trend as was obtained for pentadecane.

Diffusivities of pentadecane and heptane increase with increasing specific surface area, meso- and microporous volume (Figs. 7a−7c), which can be expected. It was reported in [28] that heptane diffusion is controlled by micropore diffusion, which is in line with the current results. Diffusivity of heptane was also increasing with increasing Lewis acid site concentration, while it was not the case for pentadecane diffusion (Fig. 7d). This result differs from the results of [29], where it was stated that lower diffusivities can be obtained with more acidic zeolites due to strong interactions with the hydrocarbon and acid sites of zeolites. No clear correlation with Brønsted acid site concentration was observed.

The diffusivities presented above are measured by complete filling the pores with liquids (heptane, pentadecane), leaving the interparticle space empty. This approach is commonly used in the literature [15]. However, it is difficult to assess effects on diffusivity measurements that can arise when the pores are filled with liquids only partially. The level of pore filling is quite difficult to control. The partial filling can potentially lead to unexpected effects such as overestimation of measured diffusivities due to a faster transport in

vapors or other more complex phenomena (see discussion of [10] in [30]). At the same time, the presence of a free liquid in the space between particles makes the analysis of the results to be more complicated. Laplace inversion [22−24] can be tried to discriminate between diffusivities in selected H-Beta-25 catalyst samples was probed by full immersion of the materials into pentadecane, for comparison.

The Laplace inversion of the measured data provided diffusion coefficient distribution curves. Two distinguishable sites corresponding to distribution maxima at ~D values of ~1×10^{-10} and 4×10^{-10} m^2/s were observed only for Bindzil (**1**).

In all other cases the components for bulk pentadecane (b-pentadecane) and pore pentadecane are not resolved. The presence of the slow diffusion component for **1** indicates restricted displacement of pentadecane inside that sites, and, likely, inefficient exchange between the bulk and this relatively isolated pool. These sites are marked as isolated pores (i-pores) in Fig. 8 curve *1* and in the text below. For H-Beta-25 (**2**) only one peak is observed (Fig. 8), indicating that this catalyst has distinguishable diffusional transport characteristics as compared to Bindzil (**2**). The peak at ~4×10^{-10} m^2/s was present for all samples, including also the reference pure pentadecane, meaning that the difference in apparent diffusion coefficients between bulk pentadecane and pentadecane in the porous materials. One has to keep in mind that Laplace inversion is an ill-posed problem, which can lead to erroneous results. At the same time, it should provide an acceptable qualitative result, indicating that the diffusion in the free liquid and in pores are of the same
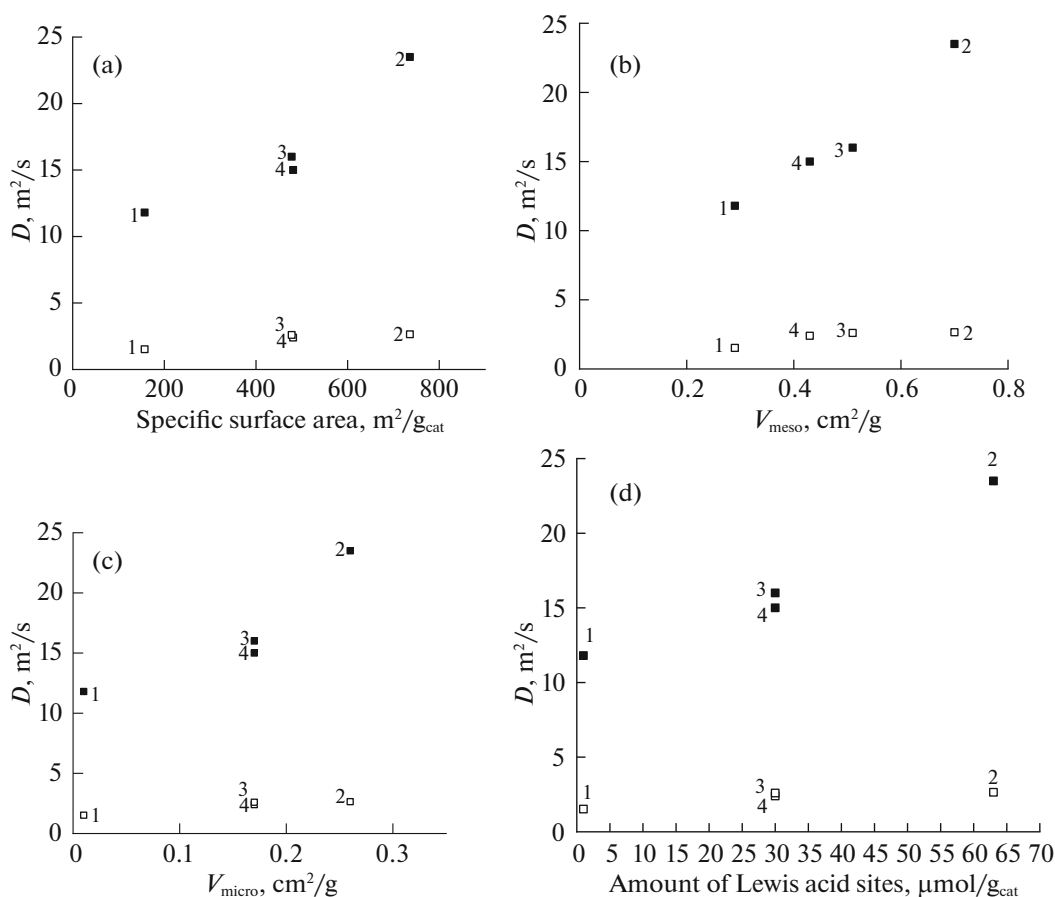
Fig. 7. Diffusivity as a function of (a) specific surface area, (b) mesoporous, and (c) microporous volume, and (d) total concentration of Lewis acid sites. Notation: heptane (■) and pentadecane (□). Numbers are the same as noted in experimental part.

order of magnitude. The width of the peak for **2** is actually broader and slightly shifted towards lower diffusion values in the case of porous materials, demonstrating the influence of the porous matrix. This observation shows that the exchange transport between the open pores (o-pores) and bulk pentadecane (b-pentadecane) is fast, compared to the observation time ($\Delta = 180$ ms). This peak most likely contains information about both o-pores and b-pentane. For instance, the correlation of transverse relaxation (T_2) and diffusion confirms this assumption for Bindzil (**1**) (Fig. 9), demonstrating the presence of three sites for this material.

In this map T_2 dimension splits the peak at ~4 × 10^{-10} m²/s into two peaks with shorter and longer T_2 values. The plausible interpretation is that the short T_2 component corresponds to pentadecane in o-pores and the longer one corresponds to b-pentadecane. The relaxation time dimension allowed separation of these peaks, which was not possible using only the diffusion measurements. It can be concluded that the apparent diffusion coefficients in o-pores and in b-pentadecane do not differ significantly from each

other. One, however, must bear in mind that the diffusion in restricted medium is not Gaussian in the general case [22]. Laplace inversion technique, in fact, uses the assumption of Gaussian diffusion propagator, which can generate erroneous results thus calling for extra caution while interpreting the results. The data presented in Fig. 5 should be considered in the first place to discuss the diffusion transport, as they were obtained by analysis of the second moment of the average diffusion propagator [22], and can be thus considered as more robust. At the same time, the Laplace inversion can be used to support that results.

When relating diffusion information to catalytic properties, it can be pointed out that the effective diffusion coefficient is directly proportional to the true diffusivity according to [31]:

$$D_e^\infty = \frac{\varepsilon}{\eta} D^0, \tag{2}$$

in which ε is porosity of the catalyst and η tortuosity. Subsequently, the data measured at room temperature can be correlated with the catalytic data obtained at higher temperatures because the order of the values remains the same. NMR diffusometry allows probing
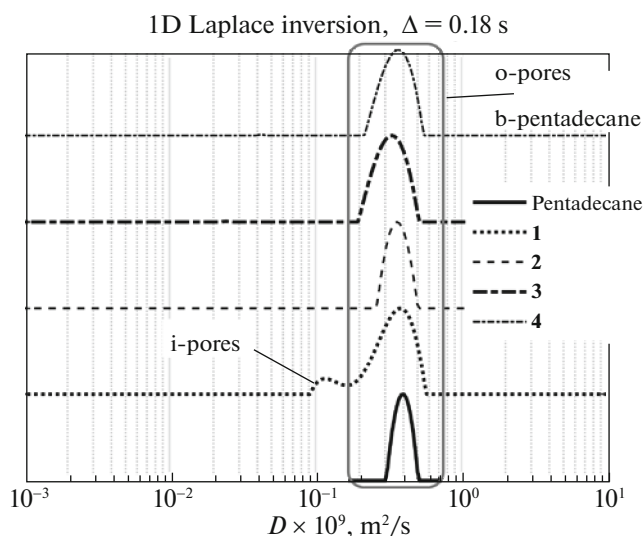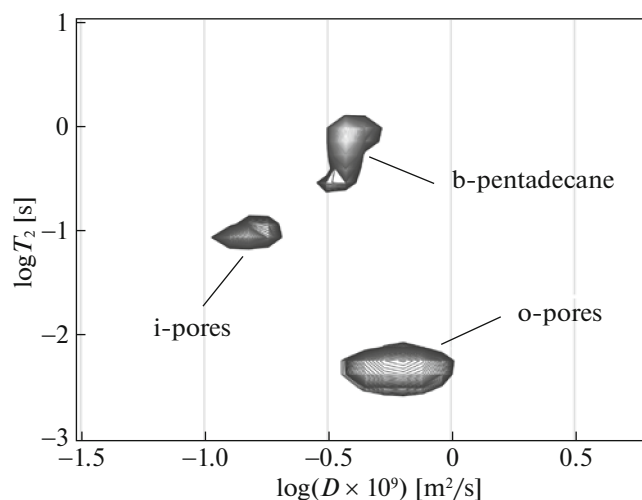
Fig. 8. Apparent diffusion coefficient distributions, as measured for bulk pentadecane and porous materials under study. A 180 ms displacement time (the time for which pentadecane molecules can diffuse before the detection) was used to obtain these data. Notation: (**1**) Bindzil, (**2**) H-Beta-25, (**3**) H-Beta-25–30 wt % Bindzil powder and (**4**) H-Beta-25–30 wt % Bindzil extrudates.

Fig. 9. A T_2-D map obtained by two-dimensional Laplace inversion for Bindzil (**1**) that demonstrates the presence of three distinguishable pools of pentadecane in this porous material. Notation: open pores denote o-pores, b-pentadecane is bulk pentadecane.

information about restrictions (borders) and tortuosity in the porous medium by variation of the observation time Δ [22, 23]. The corresponding diffusion distributions as a function of Δ show that the combined o-pores/b-pentadecane diffusion peak at around 4 × 10^{-10} m²/s is independent from the displacement time (Fig. 10), meaning that molecules in that sites effectively do not feel the porous restriction medium but rather characterize connectivity and tortuosity.

Indeed, the variation of time Δ from 150 to 1000 ms gives about the same result as the experiments with 20 ms diffusion time. Therefore, the provided diffusion coefficient in Figs. 5 and 6 (Δ = 200 ms) are estimates of effective diffusion coefficients at infinite diffusion times D_e^∞. Assuming D^0 is equal to the diffusion coefficients of bulk unrestricted liquids, the measured diffusion coefficients can be used to estimate the ε/η ratio (Eq. (2)) that are shown in Table 3. Both pentadecane and heptane provided very similar values, demonstrating independence of this parameter from the molecular size.

Interestingly, the i-pore sites of Bindzil (**1**) demonstrate a decrease in the diffusion coefficient with increasing displacement time, especially in extrudates **4**, revealing the influence of boundaries in that pores (Fig. 10). The lowest self-diffusivity for pentadecane in the i-pores in H-Beta-25–30 wt % Bindzil (**3**) was 5 fold higher than that in the corresponding extrudates (Figs. 10c, 10d) showing that more restrictions for pentadecane diffusivities could be observed in the extrudate than in a powder catalyst. Comparing the

ratio between $V_{\text{meso}}/V_{\text{micro}}$ from Table 1 for these two catalysts, it can be seen that this ratio is 1.2 fold higher for **3** in comparison to sample **4**, indicating that a larger portion of mesopores in H-Beta-25-Bindzil power facilitates better diffusion of pentadecane. It is clear that a specific porosity is formed during the extrusion. If needed, it is possible to estimate surface-to-volume ratio in isolated pores (i-pores) from the slope of the apparent diffusion coefficient as a function of the displacement time at low Δ values by employing analysis by Mitra et al. [32]. Such analysis was not accessible in this work due to technical reasons. It should also be kept in mind that the isolated pores (i-pores) represent only a minor site as it is visible for Bindzil (**1**) distributions (Figs. 8, 9). Noticeably, it is easy to see isolated pores (i-pores) in the powder (**3**) and extrudates (**4**) forms of H-Beta-25–30 wt % Bindzil catalysts in Fig. 10. This is reasonable, since that catalysts are made by mixing H-Beta-25 (**2**) with Bindzil (**1**), demonstrating that diffusometry can

Table 3. Experimental ε/η ratios from PFG NMR of pentadecane and heptane

Sample	ε/η	
	pentadecane	heptane
1 (P)	0.40	0.42
2 (P)	0.68	0.87*
3 (P)	0.60	0.59
4 (E)	0.56	0.55

* The sample was prepared in a different way by full immersion.
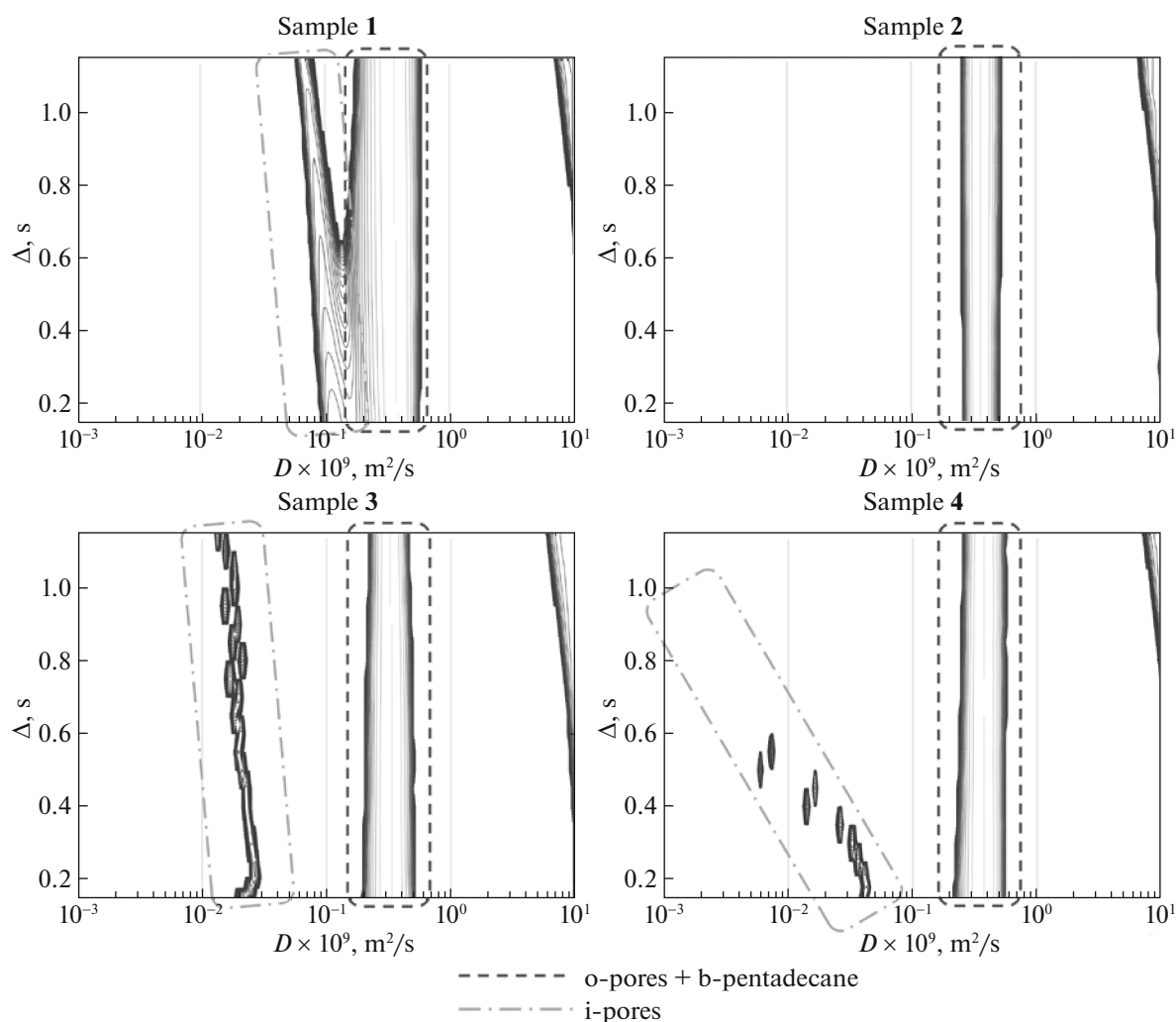
Fig. 10. Apparent diffusion coefficient distributions as a function of observation time Δ obtained by Laplace inversion for selected samples under study. The catalysts were fully immersed into the pentadecane. The peak regions corresponding to isolated pores (i-pores) and open pores (o-pores)/bulk pentadecane (b-pentadecane) are indicated with rounded rectangles. Notation: (**1**) Bindzil, (**2**) H-Beta-25, (**3**) H-Beta-25−30 wt % Bindzil powder, (**4**) H-Beta-25−30 wt % Bindzil extrudates.

use isolated pores (i-pores) as a marker of Bindzil in the studied porous materials.

4. CONCLUSIONS

Self-diffusivity of heptane and pentadecane was determined with the PFG NMR technique at room temperature for different microporous catalysts in the form of powder and extrudates. These data give valuable information about mass transfer limitations during a catalytic reaction needed for scaling-up because effective diffusivity is directly correlated with the self-diffusion coefficients. The estimates of the ratio of porosity and tortuosity are obtained from the measured D_{e}^{∞} values. The diffusivity of both heptane and pentadecane increased with increasing specific

surface area, micropore and mesopore volumes, as could be anticipated.

The diffusion experiments with materials fully immersed into pentadecane revealed sites with restricted diffusion at relatively long observation times Δ (20 up to 1000 ms), i.e., isolated pores (i-pores) only in Bindzil. The dominant peak in diffusion coefficient distributions for all samples most likely corresponds to the unresolved open pores (o-pores) and bulk pentadecane (b-pentadecane) pools. The presence of slow diffusion component in diffusion distributions is a marker of Bindzil material. Very low diffusion constants were identified especially in H-Beta-25-Bindzil extrudates, although they were of minor importance. Low diffusivities could be correlated to a low ratio of mesopore to micropore volume of H-Beta-25-Bindzil extrudates.

REFERENCES

1. M. Azkaar, Z. Vajglová, P. Mäki-Arvela, et al., Fuel **278**, 118193 (2020).

2. T. Kaka khel, P. Mäki-Arvela, M. Azkaar, et al., Mol. Catal. **476**, 110515 (2019).

3. P. Mäki-Arvela, T. A. Kaka Khel, M. Azkaar, et al., Catalysts **8**, 534 (2018).

4. M. O. Kazakov, K. A. Nadeina, I. G. Danilova, et al., Catal. Today **329**, 108 (2019).

5. M. Azkaar, P. Mäki-Arvela, Z. Vajglová, et al., React. Chem. Eng. **4**, 2156 (2019).

6. Z. Vajglová, N. Kumar, P. Mäki-Arvela, et al., Org. Proc. Res. Dev. **23**, 2456 (2019).

7. Z. Vajglová, N. Kumar, P. Mäki-Arvela, et al., Ind. Eng. Chem. Res. **58**, 18084 (2019).

8. Z. Vajglová, N. Kumar, M. Peurla, et al., Catal. Sci. Technol. **8**, 6150 (2018).

9. R. Bingre, B. Vincent, Q. Wang, et al., J. Phys. Chem. C **123**, 637 (201).

10. Z. Adem, F. Guenneau, M. A. Springuel-Huet, et al., J. Phys. Chem. C **116**, 13749 (2012).

11. H. Jobic, W. Schmidt, C. B. Krause, and J. Kärger, Microporous Mesoporous Mater. **90**, 299 (2006).

12. S. Vasenkov, W. Bohlmann, P. Galvosas, et al., J. Phys. Chem. B **105**, 5922 (2001).

13. N. Dvoyashkina, D. Freude, A. G. Stepanov, et al., Microporous Mesoporous Mater. **257**, 128 (2018).

14. W. Heink, J. Kärger, H. Pfeifer, et al., J. Chem. Soc. Faraday Trans. **88**, 3505 (1992).

15. J. Kärger, D. M. Ruthven, and D. N. Theodorou, *Diffusion in Nanoporous Materials* (Wiley-VCH, Weinheim, Germany, 2012).

16. S. K. Saxena, N. Viswanadham, and M. O. Garg, Fuel **107**, 432 (2013).

17. G. Giannetto, G. Perot, and M. Guisnet, Stud. Surf. Sci. Catal. **20**, 265 (1985).

18. J. F. Kriz, T. D. Pope, M. Stanciulescu, and J. Monnier, Ind. Eng. Chem. Res. **37**, 4560 (1998).

19. Z. Vajglová, N. Kumar, M. Peutia, et al., Ind. Eng. Chem. Res. **58**, 10875 (2019).

20. C. A. Emeis, J. Catal. **141**, 347 (1993).

21. R. M. Cotts, M. J. R. Hoch, T. Sun, and J. T. Markert, J. Magn. Reson. **83**, 252 (1989).

22. W. S. Price, *NMR Studies of Translational Motion* (Cambridge Univ. Press, Cambridge, New York, 2009).

23. P. T. Callaghan, *Translational Dynamics and Magnetic Resonance: Principles of Pulsed Gradient Spin Echo NMR* (Oxford Univ. Press, Oxford, New York, 2011).

24. V.-V. Telkki and V. V. Zhivonitko, in *Annual Reports on NMR Spectroscopy* (Academic, New York, 2019), p. 83.

25. P. Liu, Y. Yao, X. Zhang, and J. Wang, Chin. J. Chem. Eng. **19**, 278 (2011).

26. S. Hwang and J. Kärger, Adsorption (2020, in press). https://doi.org/10.1007/s10450-020-00237-0

27. H. H. Funke, A. M. Argo, C. D. Baertsch, J. L. Falconer, and R. D. Noble, J. Chem. Soc. Faraday Trans. **92**, 2499 (1996).

28. H. Zhao, J. Ma, Q. Zhang, et al., Ind. Eng. Chem. Res. **53**, 13810 (2014).

29. D. Xu, J. Ma, H. Zhao, et al., Fluid Phase Equilib. **423**, 8 (2016).

30. W.-D. Einicke, D. Enke, M. Dvoyashkin, et al., Materials (Basel) **6**, 3688 (2013).

31. D. Yu. Murzin and T. Salmi, *Catalytic Kinetics* (Elsevier, New York, 2005).

32. P. P. Mitra, P. N. Sen, L. M. Schwartz, and P. le Doussal, Phys. Rev. Lett. **68**, 3555 (1992).